

Whittle Maximum Likelihood Estimate of spectral properties of Rayleigh-Taylor interfacial mixing using hot-wire anemometry experimental data

David Pfefferlé,¹ Devesh Ranjan,² and Snezhana I. Abarzhi¹

¹*The University of Western Australia, 35 Stirling Highway, Crawley WA 6009, Australia*

²*Georgia Institute of Technology, George W. Woodruff School of Mechanical Engineering, Atlanta, GA 30332, USA*

The Rayleigh-Taylor instability (RTI) occurs in a broad range of processes in nature and technology. Analysing the power density spectrum of fluctuations in Rayleigh-Taylor (RT) flow is a means of highlighting characteristic length- and time-scales, anisotropies and anomalous processes. Raw time series from hot-wire anemometry measurements of Rayleigh-Taylor interfacial mixing experiment by Akula *et al.*, JFM **816**, 619-660 (2017) are considered as a sample case to adjust the parameters of a model power density spectrum. The results suggest that the power density spectrum of one of the flow components can be confidently modelled as the product of a power law and an exponential. The data analysis is based on Whittle's approximation of the power density spectrum for independent zero-mean near-Gaussian signals to construct a Maximum likelihood Estimator (MLE) of the parameters. Those that maximise the log-likelihood are computed numerically through Newton-Raphson iteration. The Hessian of the log-likelihood is used to evaluate the Fisher information matrix and provide an estimate of the statistical error on the obtained parameters. The Kolmogorov-Smirnov test is used to verify the hypothesis that the ratio between the observed periodogram and the estimated power density spectrum follows a chi-squared probability distribution. This step is performed to show goodness-of-fit. We also study the dependence of the model parameters on the range of mode numbers over which the fit is performed.

PACS numbers: 47.20.Ma, 47.20.-k, 52.35.-g, 52.35.Py

Keywords: Rayleigh-Taylor interfacial mixing; Whittle approximation; Maximum Likelihood Estimator; Rayleigh-Taylor instability; turbulence and turbulent spectra; Kolmogorov-Smirnov goodness-of-fit

I. INTRODUCTION

The Rayleigh-Taylor instability (RTI) develops at the interface between fluids with different densities accelerated against their density gradient [1, 2]. Intense interfacial Rayleigh-Taylor (RT) mixing of the fluids ensues with time [1–6]. Its dynamics is believed to be self-similar [1–6]. Particularly in RT mixing induced by constant acceleration, the length scale in the acceleration direction grows quadratically with time [1–6]. RTI and associated mixing play important role in a broad range of processes in nature and technology [7–9]. Examples include supernovae, inertial confinement fusion, material transformation under impact, and fossil fuel extraction [7–10]. The development of reliable methods of analysis of experimental and numerical data is required to better understand RT-relevant phenomena and to achieve a bias-free interpretation of the results [7, 11, 12].

There are several challenges in studying RTI and RT mixing: the stringent requirements on the flow implementation, diagnostics and control in experiments [7, 11–16]; the necessity to accurately capture interfaces and small-scale dissipation processes in simulations [17–20]; and the need to account for the non-local, multi-scale, anisotropic, heterogeneous and statistically unsteady character of the dynamics in theory [3, 11, 21, 22]. Furthermore, a systematic interpretation of RT dynamics from data alone is not straightforward and requires a substantial range of highly resolved temporal and spatial scales [11, 13].

Remarkable success was recently achieved in the un-

derstanding of the fundamentals of RT mixing [3, 11]. Particularly, group theory analysis found that symmetries, invariants, scaling and spectral properties of RT mixing may depart from those of isotropic homogeneous turbulence, and RT mixing may keep order, due to its strong correlations, weak fluctuations and sensitivity to deterministic conditions [3, 11]. This theory explained experiments, where the order of RT mixing was preserved even at high Reynolds numbers [5, 11, 14–16], and simulations, where departures of RT dynamics from canonical turbulent scenario were noted [17–20].

An important aspect of RT mixing that requires better understanding is the effect of fluctuations on the overall dynamics [3, 11]. The appearance of fluctuations in RT flows is usually associated with shear-driven interfacial vortical structures and with broad-band initial perturbations [3, 5, 11, 12, 14–16]. It is commonly believed that the former may produce small scale irregularities, the latter may enhance the interactions of large scales, and that both may lead RT flow to a self-similar state. Nevertheless, we still need to clearly identify the source of fluctuations in RT mixing in order to accurately quantify their properties. We also need to determine whether RT mixing is chaotic and sensitive to deterministic conditions, or whether it is stochastic and independent of deterministic conditions.

In this work, the properties of RT mixing are studied through scrupulous data analysis of experimental data, guided by group theory considerations [7, 11]. Group theory outlines the invariance-based properties of fluctuations, including their spectra and the span of

scales [7, 11, 23]. The resulting empirical model is a combination of power-law and exponential functions which describe the self-similar and scale-dependent parts of the spectrum. We process the experimental data represented by raw time series from hot-wire anemometry measurements [5]. A formal statistical method is applied to the analysis of RT mixing data (for the first time to our knowledge). The method is based on Whittle's approximation of the power density spectrum. It constructs the Maximum Likelihood Estimator (MLE) of the model parameters, numerically solves the optimisation problem through Newton-Raphson iteration algorithm, and estimates statistical errors via the use of the Fisher information matrix obtained from the Hessian of the log-likelihood. The Kolmogorov-Smirnov test [24, 25] is applied to verify the goodness-of-the-fit. We find that, in agreement with the theory, the power density spectrum of experimental quantities is confidently described by the product of a power law and an exponential.

II. DYNAMICS OF SELF-SIMILAR RT MIXING

Self-similar RT mixing has a number of symmetries, in a statistical sense, and is invariant with respect to scaling transformations. Since RT mixing is anisotropic and non-inertial, these transformations are distinct from those of isotropic inertial turbulence [3, 11, 23]. In canonical turbulence, the invariant quantity of the scaling transformation is the rate of dissipation of specific kinetic energy $\varepsilon \sim v^3/L \sim v_l^3/l$, where v_l is the velocity scale at large (small) length scale $L(l)$ [13, 26, 27]. Its invariance is compatible with the existence of an inertial interval and a normal distribution of velocity fluctuations insensitive to deterministic conditions [13, 21, 26, 27]. In RT mixing, the invariant quantities of the scaling transformation are the rate of loss of specific momentum $\mu \sim v^2/L \sim v_l^2/l$, along with the rate of gain of specific momentum $\tilde{\mu} \sim g$, in the direction of acceleration with magnitude g , with $\tilde{\mu} \sim \mu$, whereas the rate of dissipation (gain) of specific energy is time-dependent $\varepsilon(\tilde{\varepsilon}) \sim g^2 t$, where t is the corresponding time-scale [3, 11, 23].

In canonical turbulence, the invariance of the energy dissipation rate leads to the spectral density of kinetic energy fluctuations $S(k) \sim \varepsilon^{2/3} k^{-5/3}$ (or $S(\omega) \sim \varepsilon \omega^{-2}$), where $S(k)$ (or $S(\omega)$) is the spectral density and $k(\omega)$ is the wave-vector (frequency). The span of scales is constant $L/l_\nu \sim L(\varepsilon/\nu^3)^{1/4}$ where $l_\nu \sim (\nu^3/\varepsilon)^{1/4}$ is a viscous scale and ν is a kinetic viscosity [13, 26, 27]. In RT mixing, the invariance of the rate of momentum loss leads to the spectra for kinetic energy fluctuations, $S(k) \sim \mu k^{-2}$ ($S(\omega) \sim \mu^2 \omega^{-3}$) and the span of scales $L/l_\nu \sim t^2(\mu^4/\nu^2)^{1/3}$ growing with time [3, 11] $L \sim \mu t^2$, $l_\nu \sim (\nu^2/\mu)^{1/3}$.

III. RESULTS

Fitting a theoretical power density spectrum to measurements is usually approached by least-square techniques. The latter may yield biased estimators when the measurement errors are non-Gaussian. This may happen, for instance, when the data is acquired from complex non-linear and turbulent processes. Maximum-Likelihood Estimators (MLEs) may be used for providing i) an estimate of the model parameters, ii) an estimate of the standard error, iii) a fit rejection criterion to assess the match between observed and theoretical spectra. Some examples of successful use of the MLEs include: the estimate of the Batchelor cutoff wave-number in temperature gradient spectra of stirred fluid [28], peak significance testing in the periodogram of X-ray light curves of active galaxies [29], the estimate of dissipation in turbulent kinetic energy in environmental flows [30] and the spectral power density in other applications [31].

In this work, we develop an MLE-based method to analyse the raw RT data from hot wire anemometry in order to i) estimate the parameters of a theoretical power density spectrum in the form of a power law multiplied by an exponential, ii) estimate the errors on those coefficients and iii) test the statistical relevance of the fitted model against the data.

A. Theoretical model of realistic data

From the theoretical point of view, we expect a power-law spectra to be displayed over scales that are far from the largest and smallest scale, and that span a substantial dynamic range [3, 11, 13, 26, 27]. For the wave-vector $k \in (k_{min}, k_{max})$, this implies that $\lg(k_{max}/k_{min}) \gg 1$ with $k_{min} \gg K$ and $k_{max} \ll k_\nu$, where $K \sim L^{-1}$, $k_\nu \sim l_\nu^{-1}$. Similarly, for the frequency $\omega \in (\omega_{min}, \omega_{max})$, this implies that $\lg(\omega_{max}/\omega_{min}) \gg 1$ with $\omega_{min} \gg \Omega$ and $\omega_{max} \ll \omega_\nu$, where $\Omega \sim L/v$, $\omega_\nu \sim l_\nu/v_\nu$. While such conditions are easy to implement in "mathematical fluids", they are extremely challenging to achieve in experiments and simulations, where the values of K, k_ν are usually finite and bounded [5, 11, 13, 32]. Hence, one may expect the spectra to be influenced by processes occurring at scales $\sim K$ and $\sim k_\nu$. The former corresponds to long wavelengths and low frequencies, and is usually associated with some initial conditions and with effect of slow large-scale perturbations [11, 13, 26, 27, 32]. The latter requires more attention, since it is associated with fast processes at small scales. Its influence may lead to substantial departure of realistic spectra from canonical power-laws. In isotropic homogeneous turbulence, these departures are known as anomalous scalings [13, 26, 27, 32].

In experiments, we expect the dynamics to be scale-invariant at scales $k \gg k_\nu$ and be scale-dependent at scales $k \sim k_\nu$ [3, 11, 13, 26, 27, 32]. Scale-invariant functions are power-laws and logarithms, and scale-

dependent functions are exponentials [27]. An empirical function behaving as a power-law k^α for scales $k \gg k_\nu$ and as an exponential $\exp(\beta k)$ for scales $k \sim k_\nu$ has the form $S(k) \sim k^\alpha \exp(\beta k)$ (or $S(\omega) \sim \omega^\zeta \exp(\sigma \omega)$). For turbulent and ballistic dynamics, larger velocities correspond to larger length scales (smaller frequencies). This defines the signs of parameters $\alpha, \beta < 0$ (or $\zeta, \sigma < 0$). Note that the function $S(k) \sim k^\alpha \exp(\beta k)$ has already been applied in turbulence to describe realistic spectra in classical experiments and simulations [13].

In our data analysis study, we use the model function $S(k) \sim k^\alpha \exp(\beta k)$ to analyse the raw time series hot-wire anemometry data of RT interfacial mixing experiment, and adjust its parameters to the experimental power density spectrum. Details of the experiment can be found in Akula *et al.* [5] ([2017]).

B. Periodogram smoothing via Whittle MLE (spectrum fitting method)

Hot-wire anemometry is an experimental technique whereby fine temperature fluctuations are acquired at a fixed (Eulerian) position in a flowing gas stream. The change in resistance of the wire is due to heat exchange with the fluid and is some measure of the flow velocity. For isotropic, homogeneous and statistically steady flows, the measured temperature fluctuations can be viewed as fluctuations of specific kinetic energy of the fluid. This makes hot-wire anemometry a robust and reliable method of diagnostics for canonical turbulence [12, 13, 32]. RT mixing flows are anisotropic, inhomogeneous and statistically unsteady. More caution is required in the interpretation of hot-wire anemometry measurements of RT mixing flows [12]. To obtain some information on the properties of fluctuations in RT mixing, multiple wires with different orientations can be used to measure temperature (resistance) fluctuations in the direction of acceleration and in the other two transverse directions. In analogy to canonical turbulence, the measured temperature (resistance) fluctuations are labelled as fluctuations of the w , u , and v components of the Eulerian velocity field respectively.

In this work, we consider experimental data from 3-wire anemometry of RT mixing obtained at the multi-layer gas tunnel facility. The details of the experiments and the data can be found in Akula *et al.* [5] ([2017]). This paper is focused on the development of a method for analysing the data. Hence, we consider only one component of the flow, namely the v component. The comparative study of fluctuations of RT mixing and the interpretation of experimental data is conducted elsewhere.

The experimental data come in the form of $N \sim 50,000$ reals X_0, \dots, X_{N-1} recorded at constant sampling intervals Δ_t in time, see Figure 1. The signal consists of a zero-mean stationary times series with one-sided power spectral density $S(f)$. In particular, the joint marginal distribution of any part of the series is assumed to be the

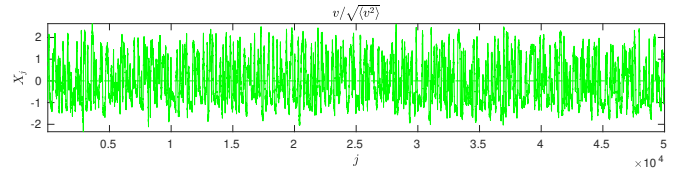


Figure 1. Experimental time series for the normal component v of the flow. The data is normalised by the standard deviation.

same as any other part with the same length[33].

For N even, we compute the discrete Fourier transform (DFT) as the list of complex numbers $\tilde{X}_1, \dots, \tilde{X}_{N/2-1}$,

$$\tilde{X}_k = \sum_{j=0}^{N-1} X_j e^{-2\pi i j k / N}. \quad (1)$$

The zeroth Fourier coefficient vanishes $\tilde{X}_0 = \sum_j X_j = 0$ because only the fluctuating part is considered. The periodogram consists of the list of reals $I_k = |\tilde{X}_k|^2 / N$, $k = 1, \dots, N/2 - 1$, see Figure 2.

For an easier graphical comparison between signals with presumably different length-scales, the data is normalised by the standard deviation and the periodogram by the data variance. The latter is motivated by the following property of the DFT

$$\langle X^2 \rangle \sim \sum_{n=0}^{N-1} \frac{X_n^2}{N} = \sum_{k=0}^{N/2-1} \frac{2I_k}{N} \Rightarrow \bar{I} := \frac{I}{\frac{N}{2} \langle X^2 \rangle}. \quad (2)$$

This normalisation is not enforced in the fitting procedure because the true variance is unknown.

We presume that, under suitable conditions [34], each Fourier coefficient \tilde{X}_k forms a pair of normally distributed random variables whose variances are approximately equal to the power spectral density, $\text{Var}(\text{Re}(\tilde{X}_k)) = \text{Var}(\text{Im}(\tilde{X}_k)) = S(k)$. The periodogram may thus provide an estimate of the power spectral density such that, for a fixed mode number k , the ratio

$$Y_k := \frac{2I_k}{S(k)} \stackrel{d}{\sim} \chi_2^2, \quad p(I_k) = p_{\chi_2^2}(Y_k) \frac{2}{S(k)} = \frac{e^{-I_k/S(k)}}{S(k)}, \quad (3)$$

is approximately distributed as a chi-square random variable with 2 degrees of freedom[34]. Furthermore, the list $\{Y_k\}_{k=1}^{N/2-1}$ forms a collection of (heteroskedastic) random variables that are approximately independent, i.e. $\text{Cov}(Y_k, Y_{k'}) \rightarrow 0$ as $N \rightarrow \infty$ for $k \neq k'$. Whittle [35] exploited the asymptotic behaviour of the periodogram to construct a Maximum Likelihood Estimator (MLE) based on the following quasi-likelihood function, over the range of mode numbers $k = k_l, \dots, k_r$,

$$\ln \mathcal{L}(S; k_l, k_r | X_0, \dots, X_{N-1}) = - \sum_{k=k_l}^{k_r} \left[\ln S(k) + \frac{I_k}{S(k)} \right],$$

where k_l and k_r are (arbitrary) left and right cutoffs.

As discussed in section II, we propose to model the RT component of the experimental spectrum in the form of a power law multiplied by an exponential,

$$S_{RT}(k) = Ck^\alpha e^{\beta k} = e^{\alpha \ln k + \beta k + \gamma}. \quad (4)$$

We also find useful to account for a low level of instrumental noise [28]. The power density spectrum is then modelled as

$$S = S_{RT} + S_{\text{Noise}} \quad (5)$$

where the simplest possible noise model is applied. Specifically, a constant white noise of $S_{\text{Noise}} \sim 10^{-6} - 10^{-9}$ mimics the flattening of the periodogram at high mode numbers $k > 3000$, see Figure 2.

The goal is to estimate the three parameters controlling the RT component of the spectrum. Defining the vectors $\vec{\theta} = (\alpha, \beta, \gamma)$ and $\vec{\phi}(k) = (\ln k, k, 1)$, we compute the gradient of the log-likelihood as

$$\begin{aligned} \partial_{\vec{\theta}} \ln \mathcal{L}(\vec{\theta}; k_l, k_r | X_0, \dots, X_{N-1}) = \\ - \sum_{k=k_l}^{k_r} \frac{S_{RT}(k)}{S(k)} \left(1 - \frac{I_k}{S(k)} \right) \vec{\phi}(k), \end{aligned} \quad (6)$$

as well as the Hessian as

$$\begin{aligned} \partial_{\vec{\theta}}^2 \ln \mathcal{L} =: H(\vec{\theta}) = \\ - \sum_{k=k_l}^{k_r} \frac{S_{RT}(k)^2}{S(k)^2} \left[\frac{I_k}{S(k)} + \left(1 - \frac{I_k}{S(k)} \right) \frac{S_{\text{Noise}}}{S_{RT}(k)} \right] \vec{\phi}(k) \vec{\phi}(k). \end{aligned} \quad (7)$$

The Maximum likelihood is obtained numerically through a Newton-Raphson method within 6-7 iterations. The scheme and stopping condition are

$$\hat{\theta}_{i+1} = \hat{\theta}_i - H_i^{-1} \cdot \partial_{\vec{\theta}} \ln \mathcal{L}_i \Rightarrow \hat{\theta} \text{ s.t. } \|\partial_{\vec{\theta}} \ln \mathcal{L}(\hat{\theta})\| < \epsilon \sim 10^{-15} \quad (8)$$

with the initial condition $\hat{\theta}_0$ obtained via Ordinary-Least-Squares on the log of the periodogram.

C. Error estimation

The (co)variance on the estimated parameters is bounded from below by the Fisher information matrix of the likelihood function, i.e.

$$\text{Cov}(\hat{\theta}, \hat{\theta}) \geq \mathcal{I}^{-1}(\vec{\theta}) \approx -\frac{H^{-1}(\hat{\theta})}{N}. \quad (9)$$

The error on the model parameters is thus estimated as $\hat{\theta} \pm \sigma$, where $\sigma_i = \sqrt{-H_{ii}^{-1}/N}$.

D. Goodness-of-fit

We apply the Kolmogorov-Smirnov (KS) test [24, 25] to determine whether the alternative hypothesis has statistical significance under the null hypothesis. Our null hypothesis is that the ratio between the observed periodogram and the model power density spectrum is distributed according to a chi-squared distribution with 2 degrees of freedom, $Y_k = \frac{2I_k}{S(k)} \stackrel{d}{\sim} \chi_2^2$. Departure from the assumed behaviour is detected through the KS test by quantifying the probability, p_{KS} , that discrepancies are due only to statistical uncertainty. In the event p_{KS} is too low, the discrepancies cannot be explained by uncertainty and so the null hypothesis is unlikely (rejected).

In detail, the Empirical Distribution Function (EDF) of the $\eta = k_r - k_l + 1$ ordered observations $Y_1 < Y_2 < \dots < Y_\eta$,

$$F_\eta(x) = \frac{1}{\eta} \sum_{k=1}^{\eta} \mathbf{1}_{(-\infty, x]}(Y_k), \quad \mathbf{1}_A(z) := \begin{cases} 1 & z \in A \\ 0 & z \notin A \end{cases} \quad (10)$$

is compared to the chi-squared Cumulative Distribution Function (CDF) $P_{\chi_2^2}$. The maximum absolute difference between the two distributions,

$$D_\eta := \sup_x |F_\eta(x) - P_{\chi_2^2}(x)|, \quad (11)$$

is used as a test statistic. Under the null hypothesis, the value $\sqrt{\eta} D_\eta$ is a random variable distributed asymptotically according to the so-called Kolmogorov distribution [36], i.e. $\sqrt{\eta} D_\eta \xrightarrow{\eta \rightarrow \infty} K$. The null hypothesis is rejected if the distance is larger than the critical value at the significance level α . In other words, given a significance level of $\alpha = 5\%$ (as per the usual convention), one computes the critical value K_α for which the random variable $\sqrt{\eta} D_\eta$ should remain inferior to in $1 - \alpha = 95\%$ of the time. If the observed data is such that

$$\sqrt{\eta} D_\eta > K_\alpha, \quad \Pr(K \leq K_\alpha) = 1 - \alpha, \quad (12)$$

then accepting the MLE fit consists of a type II error.

The p -value of the test $p_{KS} := P(K \geq \sqrt{\eta} D_\eta)$ quantifies the probability under null hypothesis of witnessing a discrepancy greater or equal than that observed. We interpret a high value of $p_{KS} > 5\%$ to indicate a consistent MLE fit. A low value of p_{KS} is interpreted as an inconsistency of the fitting assumptions with the data in regards to (i) the noise model; (ii) the left and right cutoffs, k_l and k_r ; (iii) the stationarity of the time series. The p -value will be quoted in the results as a measure of goodness-of-fit.

IV. PROPERTIES OF RT DATA

A. Spectral properties of experimental data

Figure 2 shows the periodogram computed from the times series in Figure 1 characterising fluctuations in

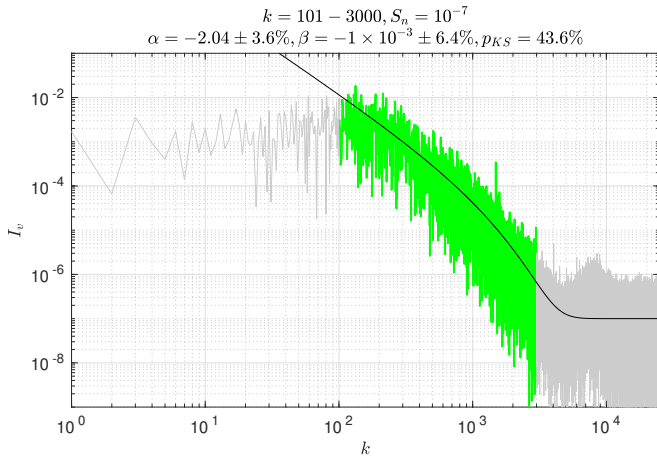


Figure 2. Periodogram of the v components of the RT flow rate on a log-log scale (normalised by the data variance). The black line is the resulting fit from the MLE of the power law and exponential decay rate coefficients α and β over a broad range of mode numbers $k = 101 - 3000$, assuming a noise level of $S_{\text{Noise}} = 10^{-7}$. Grey-coloured data points were excluded from the fit.

the normal component v of the flow. The black line in this Figure represents the model power density spectrum, whose parameters are adjusted through the fitting procedure described in section III B. For this particular MLE fit, a broad range of mode numbers $k = 101 - 3000$ is selected. The “active” modes are highlighted by colouring the data in green. The grey data depicts the amplitudes of the periodogram that have been excluded from the fit. The end “tail” of the periodogram beyond $k > 4000$ predominantly reflects instrumental noise. The fitted power density spectrum becomes flat above $k > 4000$ due to the choice of noise level at $S_{\text{Noise}} = 10^{-7}$. This adjustable parameter acts effectively as a cutoff by reducing the importance of amplitudes below S_{Noise} in the MLE. S_{Noise} is selected to be visually consistent with the data.

At high mode numbers, an exponential behaviour is revealed by the non-vanishing β coefficients. This exponential behaviour is even more prominent from the strong linear correlation between k and $\ln S_{RT}(k) \sim \beta k$ on a lin-log scale (not shown here). The associated characteristic length-scale corresponds to $k \sim 1/\beta \sim 1000$, which is much lower than both the right fitting limit ~ 3000 and the instrumental noise beyond $k > 4000$. This indicates that the corresponding length-scale is a physical feature of the flow.

At low mode numbers, the power-law dominates over the exponential term. The fitted power density spectrum thus approaches a line with slope α in log-log scale. Below $k < 70$ however, the fit significantly overestimates the periodogram, as seen through the rise of the black line well above the data points. This departure can be interpreted in several ways. Possible interpretations include: the statistical unsteadiness of the flow, sensitivity to deterministic conditions, presence of zonal com-

ponents, experimental bias, etc. This behaviour is consistent with sensitivity of the dynamics to some initial conditions at very large length scales (small mode numbers) and with the exponential character of spectra in deterministic chaos.

From the data analysis point of view, there is an arbitrariness in defining the left limit k_l of the mode number range. The effect of the mode number range on the parameter estimation is discussed in more detail in section IV C. Briefly, the α coefficient from the MLE fit becomes smaller in absolute value when the left limit is lowered. This may mean that the power-law loses relevance when the mode number range is extended to the left, since the flattening at low mode numbers can be achieved by the exponential term alone. The goodness-of-fit however worsens as we lower the left limit k_l . The fit must actually be rejected below $k_l < 30$ for v with fixed $k_r = 3000$.

An equivalent MLE fitting procedure can be applied to verify whether the periodogram can be described only by an exponential term or only by a power-law. While reasonable parameter estimations may result from this procedure, almost every evaluation of the goodness-of-fit leads to a rejection of the fits. This suggests that the dynamics is characterised by a power density spectrum that is at least as complicated as the product of a power-law and an exponential decay.

B. Analysis of residuals and goodness-of-fit

The procedure described in section III D is applied to the MLE fit reported in Figure 2 to assess the goodness-of-fit. The KS test returns a p -value of $p_{KS} = 43.6\% > 5\%$. The probability of witnessing a greater discrepancy between the fit and the data through statistical uncertainty is larger than the adopted rejection level of 5%; we interpret the MLE fit as being consistent/valid.

The top plot of Figure 3 shows the details of the goodness-of-fit procedure by comparing the empirical cumulative distribution function of the collections of ratios $Y_k = 2I_k/S(k)$ (solid coloured curve) and the chi-squared CDF (dashed black curve). The difference between the graphs is almost imperceptible. The coloured curve on the bottom plot of Figure 3 is the absolute maximum difference between the empirical and chi-squared CDF and the dashed line represents the critical value from the KS statistics $D_{5\%} \sim 2.5 \times 10^{-2}$ beyond which the MLE fit must be rejected. As seen on Figure 3, the dashed line is not exceeded.

C. Scan of left and right mode number limits

In this section, we study the dependence of the MLE fit on the range of mode numbers, particularly on the left and right cutoffs, k_l and k_r respectively.

Figure 4 shows that the power-law index varies between -3 and 0 as a function of the left and right win-

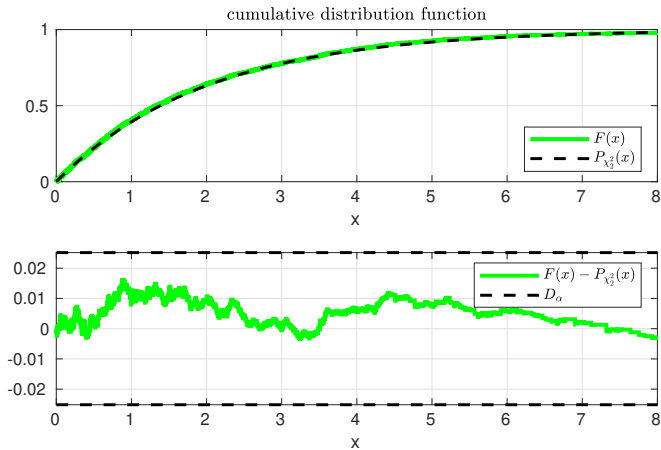


Figure 3. KS test comparing empirical cumulative distribution function of $Y_k = 2I_k/S(k)$ with chi-square CDF for MLE fit of Figure 2. The dashed black lines in the second row highlight the critical value of the absolute maximum difference at 5% significance level.

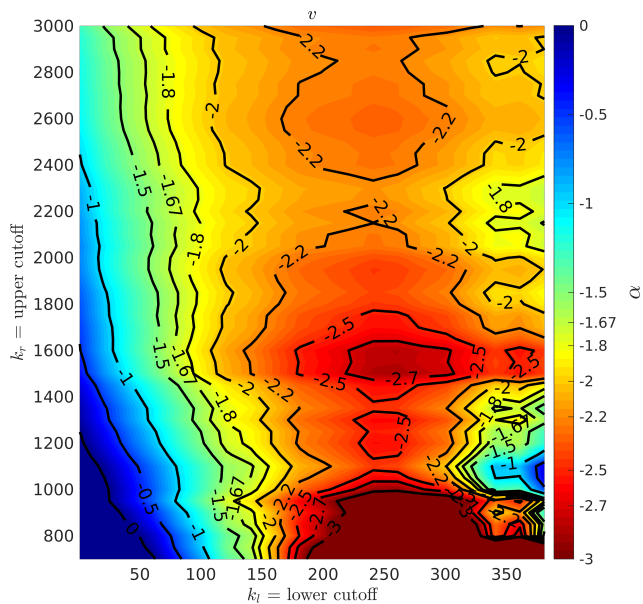


Figure 4. Dependence of the estimated power law exponent α on the left and right cutoffs for the v -component of the velocity.

dow limits k_l and k_r . For a fixed upper limit k_r , the power-law index almost vanishes when the lower limit k_l is low, which is explained by the fact that the periodogram flattens between 1 – 100 on a log-log scale and only the exponential term may generate this behaviour. The power-law index decreases to around -2.25 as the left cutoff k_l is raised to $k_l \approx 180$. Beyond this value, the evolution of α depends on the right cutoff k_r ; α becomes even more negative if the right limit is below 1100 or in the range of 1400 – 1700, but stays constant if the mode

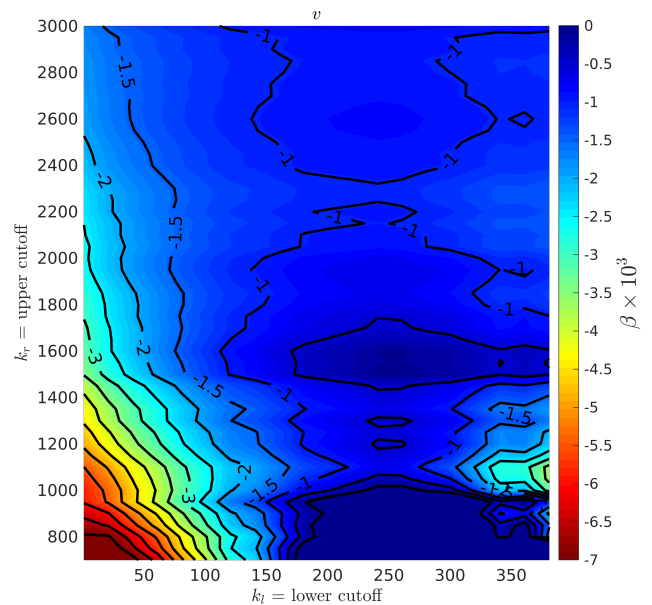


Figure 5. Dependence of the estimated exponential decay coefficient β on the left and right cutoffs for the v -component of the velocity.

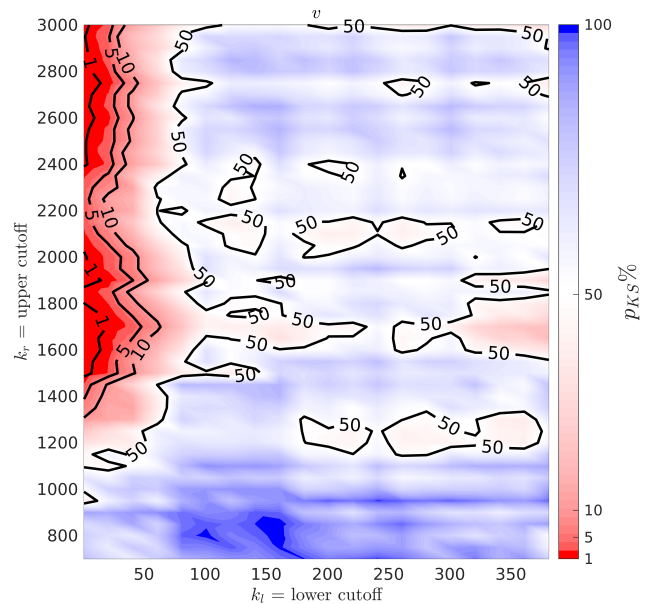


Figure 6. Dependence of the KS-test p_{KS} -value on the left and right cutoffs for the v -component of the velocity.

number range is 2000 – 2400.

On Figure 5, the exponential decay rate is shown to vary as a function of the mode number window inversely to the power-law index, reaching values between -7×10^{-3} and 0. The α and β estimates being positions of maximum likelihood, their variation is correlated with

respect to changes in parameters such as k_l and k_r . The correlation can be understood by considering the log of the power density spectrum $\ln S_{RT} = \alpha \ln k + \beta k + \gamma$ as the weighted sum of the three basic functions $\ln k$, k and 1, where the power-law has an influence on the exponential term and vice-versa under the projection method that is MLE.

Figure 6 displays the variation of the p -value of the KS test. The rejection region extends to a nearly rectangle bound by $k_l < 80$ and $k_r > 1300$.

V. DISCUSSION

We have studied the spectral properties of Rayleigh-Taylor mixing by analysing experimental hot-wire anemometry data, Figures 1-6. Guided by group theory, we have developed a formal statistical procedure for fitting the parameters of a given model power density spectrum to experimental time series, Eqs. (1-12). The method applies Maximum-Likelihood Estimation to evaluate the model parameters, the standard error and the goodness-of-fit. For the latter, the Kolmogorov-Smirnov test has been employed. The instrumental noise at the high-end of the spectrum has been incorporated into the model through a low level of white noise. The dependence of the fit parameters on the range of mode numbers, particularly on the left and right cutoffs, has been thoroughly investigated. We have considered the sensitivity of the parameter estimations to the span of scales, the left and right cutoffs, and the choice of noise level, Figures 1-6.

Bias-free methods of analysis and systematic interpretation of experimental and numerical data is necessary to “get knowledge from the data” of Rayleigh-Taylor mixing and to better understand Rayleigh-Taylor-relevant phenomena in nature and technology [3]. Our work is the first (to the authors’ knowledge) to approach this task [7]. Our analysis of hot-wire anemometry data finds that the power density spectrum of experimental quantities is confidently described by the product of a power-law and an exponential, Figures 1-6. In the self-similar sub-range, Rayleigh-Taylor spectra are steeper than those of canonical turbulence, suggesting that RT mixing has stronger correlation and weaker fluctuations when compared to canonical turbulence. In the scale-dependent sub-range, the spectra are exponential rather than power-law, suggesting chaotic rather than stochastic behaviour of the

fluctuations in Rayleigh-Taylor mixing. These results agree with group theory analysis [3, 11, 21–23]. They are also consistent with the existence of anomalous scaling in realistic experimental spectra of canonical turbulence [13, 32].

Our analysis of the experimental hot-wire anemometry data has applied a number of assumptions, Eqs. (1-12). Particularly, the spectrum of fluctuations is an accurate diagnostics of statistically steady turbulence, whereas Rayleigh-Taylor mixing is statistically unsteady [3, 11, 13, 21–23]. Fluctuations in the wire resistance can be viewed as fluctuations of specific kinetic energy in canonical turbulence; a more accurate consideration is required for Rayleigh-Taylor mixing with strongly changing scalar and vector fields [5, 12, 13]. Maximum-likelihood estimations impose strong requirements on statistical properties of times series; these requirements are challenging to obey in Rayleigh-Taylor mixing [3, 7, 11, 33–36]. The Kolmogorov-Smirnov test reliably quantifies goodness-of-fit in a multi-parameter system fluctuating about its mean; more caution is required to quantify goodness-of-fit of fluctuations (in a sense - a noise of the noise) [3, 7, 11, 24, 25]. Further developments are in demand on the fronts of experiment, theory, simulation and data analysis, in order to better understand the statistical properties of realistic non-equilibrium processes, such as anisotropic, inhomogeneous, statistically unsteady Rayleigh-Taylor mixing [3, 7, 11–13].

Note that the technique presented in this work may require alterations to treat filtered and processed signals, since it relies on (i) the canonical relation between the Fourier coefficients of a zero-mean stationary time series and its power spectral density; (ii) the asymptotic independence of the signal’s covariance matrix as a function of mode number Eqs. (1-12).

To conclude, we have developed a method of analysis of spectral properties of Rayleigh-Taylor mixing from raw hot wire anemometry experimental data, and have found that, in agreement with the theory, the power density spectrum of experimental quantities is confidently described by the product of a power-law and an exponential.

ACKNOWLEDGMENTS

The authors thank for support the University Of Western Australia (AUS), the National Science Foundation (USA), and the Department of Energy (USA).

-
- [1] J. W. Rayleigh, Proceedings of the London Mathematical Society **s1-14**, 170 (1883).
 - [2] R. M. Davies and G. I. Taylor, Proceedings of the Royal Society of London. Series A. Mathematical and Physical Sciences **200**, 375 (1950).
 - [3] S. I. Abarzhi, Philosophical Transactions: Mathematical,

- Physical and Engineering Sciences **368**, 1809 (2010).
- [4] E. E. Meshkov, *Studies of hydrodynamic instabilities in laboratory experiments* (Sarov, FGUC-VNIIEF, ISBN 5-9515-0069-9, in Russian, 2006).
- [5] B. Akula, P. Suchandra, M. Mikhaeil, and D. Ranjan, Journal of Fluid Mechanics **816**, 619–660 (2017).

- [6] B. Akula and D. Ranjan, *Journal of Fluid Mechanics* **795**, 313–355 (2016).
- [7] S. I. Abarzhi, S. Gauthier, and K. R. Sreenivasan, *Philosophical Transactions of the Royal Society A: Mathematical, Physical and Engineering Sciences* **371**, 20120436 (2013).
- [8] W. D. Arnett, *Supernovae and Nucleosynthesis: An Investigation of the History of Matter, from the Big Bang to the Present*, Princeton Series in Astrophysics (Princeton University Press, 1996).
- [9] S. W. Haan, J. D. Lindl, D. A. Callahan, D. S. Clark, J. D. Salmonson, B. A. Hammel, L. J. Atherton, R. C. Cook, M. J. Edwards, S. Glenzer, A. V. Hamza, S. P. Hatchett, M. C. Herrmann, D. E. Hinkel, D. D. Ho, H. Huang, O. S. Jones, J. Kline, G. Kyrala, O. L. Landen, B. J. MacGowan, M. M. Marinak, D. D. Meyerhofer, J. L. Milovich, K. A. Moreno, E. I. Moses, D. H. Munro, A. Nikroo, R. E. Olson, K. Peterson, S. M. Pollaine, J. E. Ralph, H. F. Robey, B. K. Spears, P. T. Springer, L. J. Suter, C. A. Thomas, R. P. Town, R. Vesey, S. V. Weber, H. L. Wilkens, and D. C. Wilson, *Physics of Plasmas* **18**, 051001 (2011).
- [10] N. Peters, *Turbulent Combustion*, Cambridge Monographs on Mechanics (Cambridge University Press, 2000).
- [11] S. I. Anisimov, R. P. Drake, S. Gauthier, E. E. Meshkov, and S. I. Abarzhi, *Philosophical Transactions of the Royal Society A: Mathematical, Physical and Engineering Sciences* **371**, 20130266 (2013).
- [12] S. S. Orlov, S. I. Abarzhi, S. B. Oh, G. Barbastathis, and K. R. Sreenivasan, *Philosophical Transactions of the Royal Society A: Mathematical, Physical and Engineering Sciences* **368**, 1705 (2010).
- [13] K. R. Sreenivasan, *Proceedings of the National Academy of Sciences of the USA* (2018), 10.1073/pnas.1800463115.
- [14] E. E. Meshkov, *Philosophical Transactions of the Royal Society A: Mathematical, Physical and Engineering Sciences* **371**, 20120288 (2013).
- [15] H. F. Robey, Y. Zhou, A. C. Buckingham, P. Keiter, B. A. Remington, and R. P. Drake, *Physics of Plasmas* **10**, 614 (2003).
- [16] B. A. Remington, H.-S. Park, D. T. Casey, R. M. Cavallo, D. S. Clark, C. M. Huntington, C. C. Kuranz, A. R. Miles, S. R. Nagel, K. S. Raman, and V. A. Smalyuk, *Proceedings of the National Academy of Sciences of the USA* (2018), 10.1073/pnas.1717236115.
- [17] J. R. Ristorcelli and T. T. Clark, *Journal of Fluid Mechanics* **507**, 213–253 (2004).
- [18] J. Glimm, D. H. Sharp, T. Kaman, and H. Lim, *Philosophical Transactions of the Royal Society A: Mathematical, Physical and Engineering Sciences* **371**, 20120183 (2013).
- [19] K. Kadau, J. L. Barber, T. C. Germann, B. L. Holian, and B. J. Alder, *Philosophical Transactions of the Royal Society A: Mathematical, Physical and Engineering Sciences* **368**, 1547 (2010).
- [20] D. L. Youngs, *Philosophical Transactions of the Royal Society A: Mathematical, Physical and Engineering Sciences* **371**, 20120173 (2013).
- [21] S. I. Abarzhi, A. Gorobets, and K. R. Sreenivasan, *Physics of Fluids* **17**, 081705 (2005).
- [22] S. I. Abarzhi, *Philosophical Transactions of the Royal Society A: Mathematical, Physical and Engineering Sciences* **368**, 1809 (2010).
- [23] S. I. Abarzhi, A. K. Bhowmick, A. Naveh, A. Pandian, N. C. Swisher, R. F. Stellingwerf, and W. D. Arnett, *Proceedings of the National Academy of Sciences of the USA* (2018), 10.1073/pnas.1714502115.
- [24] A. N. Kolmogorov, *Giornale dell’Istituto Italiano degli Attuari* **4**, 83 (1933).
- [25] N. Smirnov, *Ann. Math. Statist.* **19**, 279 (1948).
- [26] A. Kolmogorov, *Akademiia Nauk SSSR Doklady* **30**, 301 (1941).
- [27] L. Landau and E. Lifshitz, *Course of theoretical physics*, Vol. I-X (Elsevier Science, 1987).
- [28] B. Ruddick, A. Anis, and K. Thompson, *Journal of Atmospheric and Oceanic Technology* **17**, 1541 (2000).
- [29] Vaughan, S., *A&A* **431**, 391 (2005).
- [30] C. E. Bluteau, N. L. Jones, and G. N. Ivey, *Limnology and Oceanography: Methods* **9**, 302 (2011).
- [31] N. Choudhuri, S. Ghosal, and A. Roy, *Journal of the American Statistical Association* **99**, 1050 (2004).
- [32] K. R. Sreenivasan, *Rev. Mod. Phys.* **71**, S383 (1999).
- [33] A. Contreras-Cristán, E. Gutiérrez-Peña, and S. G. Walker, *Communications in Statistics - Simulation and Computation* **35**, 857 (2006).
- [34] D. Brillinger, *Time Series: Data Analysis and Theory*, Classics in Applied Mathematics (Society for Industrial and Applied Mathematics, 2001).
- [35] P. Whittle, *Journal of the Royal Statistical Society* **19**, 38 (1957).
- [36] F. J. Massey, *Journal of the American Statistical Association* **46**, 68 (1951).